

P67 Fig. 3. Strength distribution of fusion splicing.

ilar to that of fiber to fiber case, but  $A'$  is not similar because of the effects of stress concentration. Figure 3 shows the result of dynamic fatigue test. The strength distribution in liquid nitrogen consists of two regions, (I) and (II). From equation (6), it is considered that region (I) indicates the corner portion break, but region (II) indicates fiber break. By using the date of region (I), we evaluated the  $n$  and  $B$  values followed below.

$$\begin{aligned} n &= 23, \\ \log B &= -7.48, \end{aligned} \quad (7)$$

where  $B = \frac{2}{A'Y^2(n-2)K_{IC}^{n-2}}$

From above experimental results,  $n$  value is similar to that of fiber to fiber case,  $B$  value is smaller than that of fiber to fiber case.

1. Stress Intensity Factor Handbook (Y. Murakami *et al.*, (ed.)), Pergamon Press, 3, 78.
2. K. Morosawa, EDM94-33, CPM94-47, OPE94-42 (1994-08), Technical Report of IEICE.

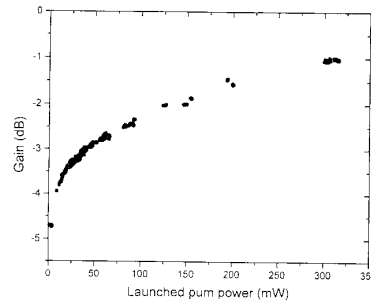
#### P68

##### Gain characterization of an $\text{Er}^{3+}$ doped phosphate glass waveguide for laser application

T. Ohtsuki, S. Honkanen,\* C-Y. Li, S. I. Najafi,\*\* N. Peyghambarian, *Optical Sciences Center, University of Arizona, Tucson, Arizona 85721*

Planar waveguide lasers and amplifiers have been demonstrated in erbium doped glasses fabricated by various techniques.<sup>1-4</sup> In addition to the low waveguide propagation loss which was realized, spectroscopic properties of the doped glasses such as emission cross section and fluorescent lifetime are also important to achieve high gain. Phosphate glass is known as an excellent rare-earth host material in terms of its large emission cross section, and the weak interaction among rare-earth ions which causes concentration quenching. Therefore, it should be possible to fabricate waveguide lasers of relatively short waveguide length with high  $\text{Er}^{3+}$  concentration. We fabricated a channel waveguide on an  $\text{Er}^{3+}$  doped phosphate laser glass (Kigre Q89) by a dry silver-film ion exchange technique,<sup>5</sup> and characterized its gain properties.

We chose  $\text{Er}^{3+}$  concentration of  $1 \times 10^{20}$  ions/cm<sup>3</sup> so that no significant concentration quenching occurs. Fluorescence lifetime measured at 1.54  $\mu\text{m}$  (8.4 ms) confirms no concentration quench-



P68 Fig. 1. Small signal gain at 1.530  $\mu\text{m}$  versus 980 nm pump power of the 1.8 cm long  $\text{Er}^{3+}$  doped phosphate glass waveguide.

ing. Ion-exchange was performed at 180°C by applying DC electric field to the silver thin films deposited on both sides of the glass with Ti/W mask. The waveguide length after end polishing was 1.8 cm. The effective refractive index of a planar waveguide measured at 632.8 nm was 1.573 for its fundamental TE mode, where the substrate index is 1.559. Small signal gain at 1.530  $\mu\text{m}$  was measured by a Ti:sapphire pump laser at wavelength of 980 nm for the channel waveguide. Figure 1 shows the gain versus pump power characteristics. Approximately 20% of the pump power was absorbed by the waveguide. Only fundamental mode was excited by the focused Gaussian laser beam of 12  $\mu\text{m}$  spot size in this multi-mode channel waveguide. The mode size of the pump and signal beam propagating in the channel waveguide was  $9 \times 2 \mu\text{m}^2$  and  $11 \times 3 \mu\text{m}^2$ , respectively. No up-conversion luminescence was observed at visible wavelength up to the maximum excitation. Waveguide propagation loss was estimated to be 0.6 dB/cm, and the inherent loss due to the  $\text{Er}^{3+}$  absorption at the signal wavelength is approximately 3.7 dB. The observed gain is comparable to the total loss at the signal wavelength used for this measurement (1.530  $\mu\text{m}$ ), since it is shorter than the wavelength of the peak emission cross section (1.535  $\mu\text{m}$ ). However, higher gain is expected at longer wavelengths, where the emission cross section is larger than the absorption cross section.

Taking into account the larger cross section ratio of the emission to the absorption at 1.535  $\mu\text{m}$ , we conclude that gain of the  $\text{Er}^{3+}$  doped phosphate glass waveguide fabricated by current method should exceed the total loss. Low threshold laser can be realized provided low propagation loss and high  $\text{Er}^{3+}$  concentration. Waveguide design for laser application will be discussed based on our experimental results, as well as the comparison of the gain characteristics with the waveguides fabricated by different methods and different material.

\*Nokia Research Center, P.O. Box 45, FIN-00211 Helsinki, Finland

\*\*Ecole Polytechnique, P.O. Box 6079, Station A, Montreal (Quebec), H3C 3A7, Canada

1. K. Hattori, *et al.*, Electron. Lett. 29, 357 (1993).
2. K. Shuto, *et al.*, Electron. Lett. 29, 139 (1993).

3. M. Nakazawa, *et al.*, Electron. Lett. 28, 2054 (1992).
4. T. Feuchter, *et al.*, IEEE Photon. Technol. Lett. 4, 542 (1992).
5. S. Honkanen, *et al.*, Electron. Lett. 27, 2167 (1991).

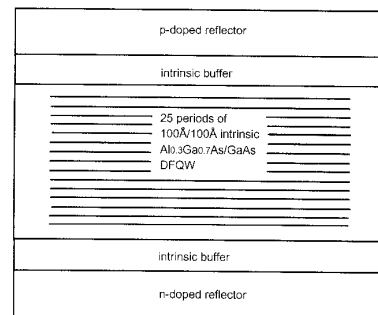
#### P69

##### Improved performance of vertical-cavity modulator through the use of diffused quantum wells

E. Herbert Li, Wallace C. H. Choy, *Department of Electrical and Electronic Engineering, The University of Hong Kong, Pokfulam Road, Hong Kong*

Normal incidence (transverse) type of multiple quantum well (MQW) optical modulator is attractive for providing a large area in coupling the light in and out of the device and application in vertical opto-electronic integrating technology.<sup>1</sup> However, this type of modulator is limited by a relatively long optical interaction path and a high driving voltage requirement. These discrepancies can be highly improved by introducing the transverse type of symmetric Fabry-Perot (FP) structure in the vertical optical cavity on a substrate, where an intrinsic-MQW layer is sandwiched between two reflectors, this will increase the effective optical interaction length and reduce the applied voltage swing.<sup>2</sup> A thermally (post-process annealing) diffused QW (DFQW)<sup>3</sup> is proposed here as an intrinsic material in the symmetric-FP vertical cavity for improving the modulator performance and to provide an operational wavelength tuning range. It is expected that this DFQWs based FP modulator will become an important candidate for the vertical integrating technology. The electro-optical property of the DFQW FP-cavity modulator is analyzed here for its transmission strength  $T$  and field induced transmission change  $\Delta T$ .

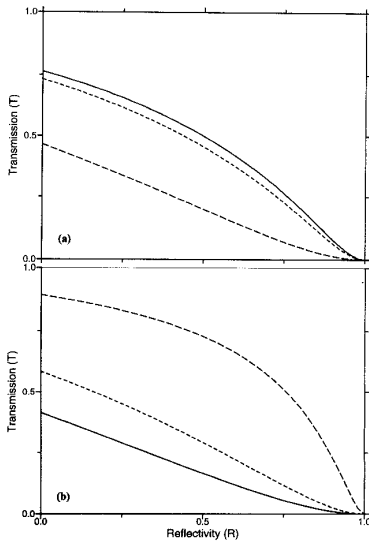
Fig. 1 shows the schematic FP device which consists of an intrinsic layer (25 periods of 100 Å/100 Å  $\text{Al}_{0.3}\text{Ga}_{0.7}\text{As}/\text{GaAs}$  DFQW) sandwiched between two buffer layers in the cavity, and followed by two reflectors with identical reflectivity  $R$  doped as a p-i-n structure for electric contacts. The extent of diffusion is characterized by a diffusion length  $L_d$  ( $L_d = 0$  represents the as-grow QW).<sup>3</sup>  $T$  and  $\Delta T$  can be determined from the absorp-



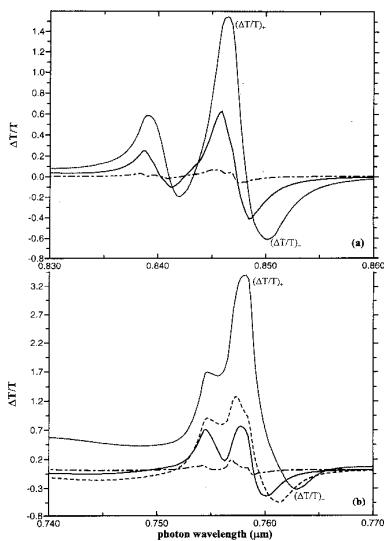
P69 Fig. 1. Schematic of the DFQWs symmetric-FP vertical cavity transmission modulator.

tion coefficient  $\alpha$ , which is calculated from a model similar to Ref. 4 without the polarization sensitivity.

It is interesting to note that the magnitude of  $\Delta T$  (between  $F = 0$  and  $50 \text{ kV/cm}$ ) is enhanced in the DFQW ( $L_d = 50 \text{ \AA}$ ) for all values of  $R$ , as compared to the  $L_d = 0$  case, at a chosen operational wavelength  $\lambda_{op} = 758 \text{ nm}$  (to obtain maximum  $\Delta T$ 's), see Fig. 2. Analysis of the modulator is based on the non-normalized  $\Delta T/T$  spectra in the normal-OFF operational mode with an optimized  $R = 0.5$  for the two  $L_d$ 's, see Fig. 3. One positive peak



**P69 Fig. 2.** The transmission  $T$  spectra as a function of reflectivity  $R$  for  $F$  ( $\text{kV/cm}$ ) = 0 (solid), 30 (dot), 50 (dash). (a)  $L_d = 0 \text{ \AA}$  at  $\lambda_{op} = 0.850 \text{ \mu m}$  and (b)  $L_d = 40 \text{ \AA}$  at  $\lambda_{op} = 0.758 \text{ \mu m}$ .



**P69 Fig. 3.** The  $\Delta T/T$  spectra for DFQWs of thickness  $d = 0.5 \text{ \mu m}$  and  $R = 0.5$  for  $F$  ( $\text{kV/cm}$ ) = 10 (dash-dot), 30 (solid), 40 (dash), and 50 (dot). (a)  $L_d = 0 \text{ \AA}$  and (b)  $L_d = 40 \text{ \AA}$ .

( $\Delta T/T$ )<sub>+</sub> and one negative trough ( $\Delta T/T$ )<sub>-</sub> can be observed in each spectrum, where the former corresponds to the largest modulation depth while the latter, although slightly smaller in magnitude, corresponds to a lower resident absorption  $\alpha(F = 0)$ . It can be seen that ( $\Delta T/T$ )<sub>+</sub> increases from 1.53 ( $L_d = 0$ ) to 3.40 ( $L_d = 40 \text{ \AA}$ ), which is an attractive feature for developing a high intensity modulator with a narrow  $\lambda_{op}$  range. Also a steady  $\Delta T/T \approx 0.6$  (without any sign change) is obtained for a range of  $\lambda_{op}$ 's (740 to 760  $\text{nm} \approx 20 \text{ nm}$ ) in the DFQW between  $F = 40$  and  $50 \text{ kV/cm}$ , therefore it can be operated as a 20 nm band-width transmission modulator with only a single DFQW structure. Finally, the ( $\Delta T/T$ )<sub>-</sub> has a wavelength range of  $\lambda_{op} = 850 - 782 \text{ nm}$  with an acceptable fluctuation of  $\Delta T/T = (0.62 - 0.54)/0.62 \approx 12\%$  for cases of  $L_d$  from 0 to 30  $\text{\AA}$ , so it can be employed as a wide band-width modulator with a multi-section consists of differential  $L_d$ 's.

1. G. A. Evan, *et al.*, IEEE J. of Quantum Electron. 27, 1594 (1991).
2. M. Whitehead, G. Parry, P. Wheatley, IEE Proc. Pt. J 136, 52 (1989).
3. E. H. Li, B. L. Weiss, Phys. Rev. B 4, 445 (1993).
4. E. H. Li, K. S. Chan, B. L. Weiss, J. Micallef, Appl. Phys. Lett. 63, 533 (1993).

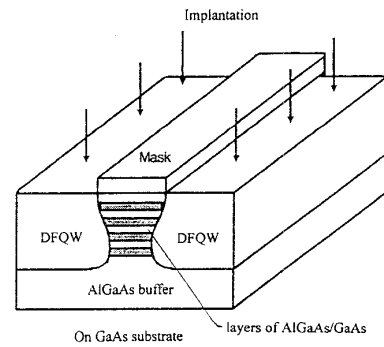
**P70**

**Impurity induced disordering produced lateral optical confinement in AlGaAs/GaAs quantum well waveguides**

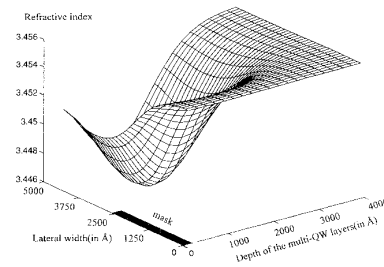
E. Herbert Li, Chun-Bong Cheung, Wai-Kin Tsui, *Department of Electrical and Electronic Engineering, The University of Hong Kong, Pokfulam Road, Hong Kong*

The impurity induced disordering (IID) technique provides an efficient way to realize waveguiding structure in optoelectronic integrated circuits.<sup>1</sup> The masked implantation process produces a modification of the quantum well (QW) material which in turn modifies its refractive index.<sup>2</sup> This creates a refractive index step between the implanted and nonimplanted regions and produces lateral confinement for photons in the lateral dimension, thus a 2-D waveguide is formed. Although there have been a lot of effort spent in studying the electronic and optical properties of the IID modified AlGaAs/GaAs QW structures, the detailed waveguiding properties of this type of devices is still not known. A detail model is considered here on the two dimensional IID waveguide structure and results indicate guiding requirements on the structure's dimension, effects on the optical confinement factor, and the wavelength requirement for single mode propagation.

The structure to be modeled consists of  $\text{Al}_{0.3}\text{Ga}_{0.7}\text{As}/\text{GaAs}$  QWs (10 to 40 periods of 100  $\text{\AA}$  wide well and barrier layers) and thick  $\text{Al}_{0.3}\text{Ga}_{0.7}\text{As}$  buffer layer grown on a GaAs substrate; the schematic of the structure is shown in Fig. 1. In our model,  $\text{Ga}^+$  ion is implanted with a projected range located around the center of the QW layers. The annealing time and temperature in the simulation is 20



**P70 Fig. 1.** Schematic of the IID multi-quantum well waveguide structure.



**P70 Fig. 2.** Refractive index profile (half symmetry) of a structure with 20 multi-QW layers, 5000  $\text{\AA}$  mask width, and propagation wavelength at  $1 \text{ \mu m}$ .

seconds and  $900^\circ\text{C}$ , respectively. In order to analyze the waveguiding properties accurately, the impurity density profile as-implanted was computed base on both experimental and simulation results.<sup>3</sup> On the basis of these initial conditions, the 2-D impurity distribution after an annealing time  $t$  was then computed by solving a non-constant coefficient diffusion equation using a finite element method. This impurity concentration profile determines the 2-D dependent diffusion coefficient and thus the position dependent diffusion length of the Al/Ga atoms at any given time can be obtained. Using a previously developed model,<sup>4</sup> a 2-D refractive index profile was then calculated from these diffusion lengths, as shown in Fig. 2. The TE mode waveguide equation was solved using a finite difference method to determine the propagation coefficient,  $\beta$ , as well as the optical electric field profile, and followed by the determination of the optical confinement factor.

The parameters of the IID waveguide structure such as the mask width,  $L_M$ , QW layer thickness,  $d$ , ion implantation energy, operational wavelengths,  $\lambda$ , were varied in order to analyze the single and multiple mode waveguiding requirements. It is found that the waveguide dimension, that is the mask width and the thickness of the multi-QW layers, should be at least half of the dimension of the propagation wavelength to provide a satisfactory wave confinement factor of  $\sim 0.5$ . In fact guiding was found to be sup-